

## Shape control of spacecraft antenna reflector using lead-free piezoelectric actuators

C.K. Susheel\*, Rajeev Kumar, Vishal S. Chauhan and Rahul Vaish

*School of Engineering, Indian Institute of Technology Mandi, 175001 Mandi, Himachal Pradesh, India*

The spacecraft antenna reflector orbiting in the space environment would be exposed to continuous variation in both temperature level and temperature distribution because of the variation of solar radiation and shadowing conditions (temperature varies from  $-80$  to  $180$  °C). The thermally induced structural responses would occur with the variations of the on-orbit thermal loads. Thermal induced deformation could adversely affect the performance of antenna reflector. The thermally induced deformation can be controlled using lead-based piezoelectric actuator. In the last few decades, these lead-based piezoelectric ceramics are used abundantly due to their superior performance. However, these lead-based piezoelectric ceramics are toxic in nature and cause severe health and environmental problems during its fabrication. In this study, thermally induced deformations in the antenna reflector are controlled using lead-free piezoelectric ceramics. Finite element formulation of layered composite antenna reflector has been presented to predict the deformation. Further beam shaping and beam steering of the antenna reflector through the piezoelectric actuator has been demonstrated. Finally active shape control of antenna reflector has been demonstrated by optimising the size and location of piezoelectric patches and the applied electric potential.

**Keywords:** finite element modelling; active shape control; lead-free piezoelectric ceramics; antenna reflector

### 1. Introduction

Spacecraft antennas are used as radars, satellite communication networks and space-borne remote sensing systems. Performance of such systems deteriorates with the distortion in their shape and surface. These distortions may get introduced due to manufacturing defects, in-orbit thermal distortion, material degradation, loose structural joints or creep as stated in Agrawal, Elshafei, and Song (1997). To keep the distortion level within prescribed limit or to retain the original shape, piezoelectric actuators are utilised for the shape control. Further these antennas have a limitation that they can provide only one particular beam pattern. Realignment of whole satellite is required if one needs to scan from one point to another or to vary beam pattern. Shape control can also help to make an antenna capable of scanning from one point to another as well as capable of changing desired coverage area without any realignment. The property of antenna which allows it to scan from one point to another without realignment is referred to as beam steering and the property which allows it to change the desired coverage area, either to increase or decrease, is referred to as beam shaping as stated by

---

\*Corresponding author. Email: [chander\\_s@students.iitmandi.ac.in](mailto:chander_s@students.iitmandi.ac.in)

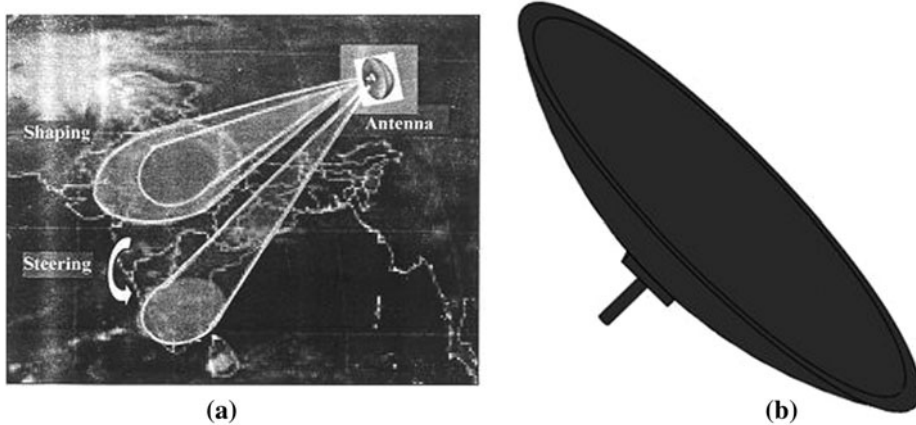


Figure 1. (a) Beam shaping and beam steering phenomenon Washington (1996). (b) General parabolic shape of antenna reflector.

Washington (1996) and depicted in Figure 1(a). A number of smart materials are available such as piezoelectric, shape memory alloys and electrostrictive materials, which may be used as actuators for shape control. Many researchers have successfully demonstrated the use of piezoelectric materials as sensors and actuators. Koconis, Kollar, and George (1994) used piezoelectric actuators in shape control of structural elements such as composite beams, plates and shells. Voltage needed to achieve desired shape was calculated analytically using two-dimensional, linear, shallow shell theory including transverse shear effects. Agrawal and Treanor (1999) presented the analytical and experimental results on optimal placement of piezoceramic actuators for shape control of beam structures. The analytical model for predicting beam deformation was based on Euler–Bernoulli model. It was found that simultaneous optimisation of the locations and input voltages of a fixed set of actuators proved to be unreliable, thus optimised actuator locations and input voltages were found separately to produce much more reliable results. A literature review is presented by Irschik (2002) for shape control of structures, where special emphasis is laid upon smart structures with piezoelectric control actuation. Haftka and Adelman (1985) introduced the concept of shape control by presenting analytical procedure for computing temperatures in control elements so as to minimise the overall distortion of large space structures from their original shape. Capabilities of piezoelectric materials are sufficiently enough for certain applications such as recovering from the effects of thermal distortion and manufacturing surface errors. Yoon and Washington (1998) developed an active aperture antenna that employs Lead zirconate titanate ( $\text{Pb} [\text{Zr}_x\text{Ti}_{1-x}] \text{O}_3$ ) (commonly known as PZT) strips as actuators. The electric field is applied to the PZT strip, which makes it to expand or contract. When joined perfectly on structure, this expansion or contraction causes the production of a bending moment which makes the structure bend. This can also help in achieving beam shaping and beam steering for antenna reflector. Agrawal et al. (1997) used higher deformation theory to develop finite element model for a composite plate with piezoelectric sensors and actuators. The voltages applied to the actuators are optimised to minimise the error between the desired shape and the deformed shape. Doubly curved antenna structure was modelled by Yoon, Washington, and Theunissen (2000) as shallow spherical shell, to achieve better performance in controlling the coverage

area. They showed that an active aperture antenna can be developed using piezoelectric actuators which can be used to change far-field radiation patterns by shape changing. Gupta (2011) carried out optimisation based on genetic algorithm (GA) to find out optimum location, length and applied electric field to the piezoelectric actuators to achieve desired steering of antenna.

In this paper, shape control of antenna reflector (Figure 1(b)) with the help of various piezoelectric materials is carried out using finite element formulation based on degenerated shell element for generally used laminated paraboloidal shell structure. The model is validated with existing literature and a numerical study is carried out for the shape control along with beam shaping and beam steering of a laminated antenna reflector under thermal loading. PZT is abundantly used as sensors and actuators, which contains 60 weight percent lead. Due to its high toxicity use of lead has been abandoned from many commercial applications and materials. Although there has been a concerted effort to develop lead-free piezoelectric ceramics, no effective alternative to PZT has yet been found. Here, an effort has been made to study some lead-free piezoceramics which can be used as an alternative for PZT.

## 2. Material and finite element methods

### 2.1. Material

In this paper, emphasis is given to replace the lead-based piezoelectric materials with environment-friendly lead-free materials. Both lead-based and lead-free materials are mostly used in transducer applications. Yasuyoshi et al. (2004), Maeder, Damjanovic, and Setter (2004), Takenaka, Nagata, and Hiruma (2008), Aksel and Jones (2010) have reported various alternatives to lead-based piezoelectric materials. Despite the concerted effort from a number of researchers to develop lead-free piezoelectric ceramics, no alternative to completely replace PZT has yet been found. In this paper following two lead-free piezoelectric materials have been selected to study their performance in comparison to PZT. One material is  $K_{.475}Na_{.475}Li_{.05}(Nb_{.92}Ta_{.05}Sb_{.03})O_3$  (KNLNTS) presented by Lee, Kwok, Li, and Chan (2009) and the other is  $.885(Bi_{.5}Na_{.5})TiO_3-.05(Bi_{.5}K_{.5})TiO_3-.015(Bi_{.5}Li_{.5})TiO_3-.05BaTiO_3$  (BNK-LBT) presented by Chan, Choy, Chong, Li, and Liu (2008). An effort has been made to use them as an alternative for PZT in beam shaping, beam steering and shape control of antenna reflectors. The reason to select only these two materials is that KNLNTS and BNK-LBT are lead-free piezoelectric materials that have comparable piezoelectric properties to PZT. Properties of these materials are given in Table 1.

### 2.2. Finite element method

In this section, finite element formulation of composite piezolaminated layered shell is presented to predict static response. The formulation is based on first-order shear deformation theory. First geometric and displacement field expressions are given, followed by piezoelectric constitutive equations and electric field expressions. Finally equations of motion are described. Figure 2(a) shows a piezolaminated composite structure having  $n$ -layers. Top and bottom piezoelectric layers act as actuators. The thickness of piezoelectric layer is very less when compared to shell structure. The piezoceramic layers are perfectly bonded above and below on shell surface and the effect of bonding material is neglected on the properties of structure. The major contribution of this paper is the study of beam shaping, beam steering and optimised shape control of parabolic

Table 1. Material property table.

Properties	Host structure	Piezo-electric materials			
		Carbon-epoxy	PZT (Lead zirconate titanate)	KN-LN-TS (Potassium sodium niobate based ceramic)	BNK-LBT (Bismuth titanate based ceramic)
Elastic moduli ( $10^9$ Pa)	$E_1$	135.2	61	87	110.5
	$E_2$	9.24	61	87	110.5
	$E_3$	9.24	61	87	110.5
Poisson ratio	$\nu_{12}$	.32	.29	.39	.278
	$\nu_{23}$	.32	.29	.39	.278
	$\nu_{31}$	.32	.29	.39	.278
Shear moduli ( $10^9$ Pa)	$G_{12} =$	6.28	23.64	31.29	43.23
	$G_{23} =$				
	$G_{13}$				
Density ( $\text{kg/m}^3$ )		1600	7700	4600	5780
Piezoelectric charge constant			$d_{31} = 171\text{e-}12$ (m/V)	$e_{31} = 16.3$ (C/m <sup>2</sup> )	$e_{31} = 3.91$ (C/m <sup>2</sup> )
			$d_{32} = 171\text{e-}12$ (m/V)	$e_{32} = 16.3$ (C/m <sup>2</sup> )	$e_{32} = 3.91$ (C/m <sup>2</sup> )
Electric permittivity ( $10^{-9}$ f/m)	$b_{11}$		16.5	5.43	2.283
	$b_{22}$		16.5	5.43	2.283
	$b_{33}$		16.5	6.6	3.929
Thermal expansion ( $10^{-6}$ m/m °C)	$\alpha_{11}$	-.30	1.2	2.96	3.8
	$\alpha_{22}$	28	1.2	2.96	3.8

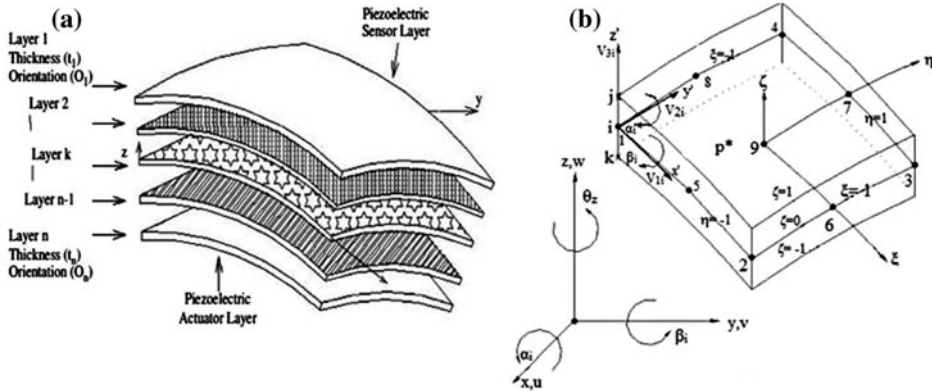


Figure 2. (a) Piezo-laminated layered shell structure. (b) Nine node degenerated shell element Kumar et al. (2008).

antenna reflector using lead-free piezoelectric materials. The theoretical and numerical formulation of both types of materials is the same. The laminated composite structures under consideration are made up of various laminae with various stacking sequence, details of which will be discussed later.

### 2.2.1. Geometry and displacement field

In the present study, nine noded degenerated shell element (shown in Figure 2(b)) has been taken into consideration for finite element formulation. The coordinates of arbitrary point within the shell can be given in terms of thickness and nodal coordinates as:

$$\begin{Bmatrix} x \\ y \\ z \end{Bmatrix} = \sum_{i=1}^{nnel} N_i \begin{Bmatrix} x_i \\ y_i \\ z_i \end{Bmatrix} + \frac{1}{2} th_i \begin{Bmatrix} l_{3i} \\ m_{3i} \\ n_{3i} \end{Bmatrix} \quad (1)$$

where  $x_i, y_i, z_i$  are the global coordinates of mid-surface node  $i$ ,  $h_i$  is the thickness of node  $i$ ,  $t$  is the thickness of shell element,  $l_{3i}, m_{3i}, n_{3i}$  are the normal unit vectors at node  $i$ ,  $N_i$  is the shape function and  $nnel$  is the No. of nodes per element.

Taking into account the shell assumptions of degeneration process, the displacement field is described by five mechanical degrees of freedom i.e. three displacements ( $u, v, w$ ) and two rotations ( $\alpha_i, \beta_i$ ). The displacement of any point within the element can be given as:

$$\begin{Bmatrix} u \\ v \\ w \end{Bmatrix} = \sum_{i=1}^{nnel} N_i \begin{Bmatrix} u_i^0 \\ v_i^0 \\ w_i^0 \end{Bmatrix} + \frac{1}{2} th_i \begin{bmatrix} l_{1i} & -l_{2i} \\ m_{1i} & -m_{2i} \\ n_{1i} & -n_{2i} \end{bmatrix} \begin{Bmatrix} \alpha_i \\ \beta_i \end{Bmatrix} \quad (2)$$

where  $l_{1i}, m_{1i}, n_{1i}$  are the direction cosines of tangent unit vector  $V_{1i}$  and  $l_{2i}, m_{2i}, n_{2i}$  are the direction cosines of tangent unit vector  $V_{2i}$ . The rotations about  $V_{1i}, V_{2i}$  are  $\alpha_i$  and  $\beta_i$ .

### 2.2.2. Piezoelectric constitutive equations (direct and converse effect)

The linear piezoelectric constitutive equations representing direct and converse piezoelectric effect are given as follows (Kumar, Mishra, & Jain, 2008).

$$\{D\}_k = [\bar{e}]_k \{\varepsilon\}_k + [\bar{b}]_k \{E\}_k + \{\bar{p}\}_k \Theta_k \quad (3)$$

$$\{\sigma\}_k = [\bar{Q}]_k \{\varepsilon\}_k - [\bar{e}]_k^T \{E\}_k - \{\bar{\lambda}\}_k \Theta_k \quad (4)$$

where  $\{D\}$ ,  $\{E\}$ ,  $\{\varepsilon\}$ ,  $\{\sigma\}$ ,  $\{p\}$  and  $\{\lambda\}$  are the electrical displacement, electric field, strain vector, stress vector, pyroelectric coefficient and stress-temperature coefficient, respectively.  $[Q]$ ,  $[e]$ ,  $[b]$  are the elastic stiffness coefficients, piezoelectric coefficient and dielectric constant matrix, respectively.

The above piezoelectric constitutive equations are in material coordinates. These equations are required to be converted to global coordinates. This can be done through transformation presented by Kumar et al. (2008).

$$\{\bar{\lambda}\}_k = [T_\varepsilon]^T [T_o]_k^T \{\lambda\}_k \quad (5)$$

$$[\bar{e}]_k = [T_v]^T [e]_k [T_o]_k [T_\varepsilon] \quad (6)$$

$$[\bar{b}]_k = [T_v]^T [b]_k [T_v] \quad (7)$$

$$[\bar{Q}]_k = [T_\varepsilon]^T [T_o]_k^T [Q]_k [T_o]_k [T_\varepsilon] \quad (8)$$

where  $[T_v]$  is the vector transformation matrix,  $[T_o]$  is the ply orientation transformation matrix and  $[T_\epsilon]$  is the strain transformation matrix.

### 2.2.3. Electric field

In the present study, it is assumed that the electric field acts in thickness direction of piezoelectric layer and electric effect is constant within a layer of element as discussed by Detwiler, Shen, and Venkayya (1995). Within an element, electric field inside  $k$ th layer can be given mathematically as:

$$\{E\}_k = -\{B_\phi\}_e \phi_{pk} \quad (9)$$

$$\{B_\phi\}_e = \frac{1}{t_{pk}} \begin{Bmatrix} l_3 \\ m_3 \\ n_3 \end{Bmatrix} \quad (10)$$

where  $t_{pk}$ ,  $\phi_{pk}$  are the thickness and electric potential of  $k$ th piezoelectric layer, respectively.

### 2.2.4. Equations of motion

The governing equations for an element can be written as (Detwiler et al. (1995))

$$[K_{uu}]_e \{q\}_e + [K_{u\phi}]_e \{\phi\}_e - [K_{u\theta}]_e \{\theta\}_e = \{F_m\}_e \quad (11)$$

$$[K_{\phi u}]_e \{q\}_e - [K_{\phi\phi}]_e \{\phi\}_e + [K_{\phi\theta}]_e \{\theta\}_e = \{F_q\}_e \quad (12)$$

where  $[K_{uu}]_e$  is the elemental elastic stiffness matrix,  $[K_{u\phi}]_e$  is the elemental elastic–electric coupling stiffness matrix,  $[K_{\phi\phi}]_e$  is the elemental electric stiffness matrix,  $[K_{u\theta}]_e$  is the elemental elastothermal stiffness matrix and  $[K_{\phi\theta}]_e$  is the elemental electrothermal stiffness matrix as given by Detwiler et al. (1995).  $\{F_m\}_e$  and  $\{F_q\}_e$  are applied mechanical force and applied electrical charge for an element, respectively.  $\{q\}_e$  is the elemental nodal displacement vector,  $\{\phi\}_e$  is the elemental voltage vector and  $\{\theta\}_e$  is the elemental temperature vector. By assembling the elemental equations, we will get global governing equations as:

$$[K_{uu}]\{q\} + [K_{u\phi}]\{\phi\} - [K_{u\theta}]\{\theta\} = \{F_m\} \quad (13)$$

$$[K_{\phi u}]\{q\} - [K_{\phi\phi}]\{\phi\} + [K_{\phi\theta}]\{\theta\} = \{F_q\} \quad (14)$$

## 3. Numerical results

### 3.1. Validation of finite element model

The finite element model presented above was first employed to reproduce the analytical results presented by Lam, Peng, Liu, and Reddy (1997) for the purpose of validation. A cantilever laminated composite plate (200 mm × 200 mm) with both the upper and lower surfaces symmetrically bonded by piezoelectric ceramics as studied by Lam et al. (1997) has been modelled. Thirty-six elements (6 × 6) are used to model the plate. The plate consists of four composite layers and two outer piezo-layers. The stacking sequence of

the composite plate is  $[-\theta/\theta/-\theta/\theta]$  and  $\theta = \pi/4$ . The total thickness of the composite plate is 1 mm and each layer has the same thickness (0.25 mm); the thickness of each piezo-layer is 0.1 mm. The effects of adhesive layers have been neglected. The plate is made of graphite–epoxy composites and the piezoceramic is PZT.

First, the voltage of  $-10$  V and  $+10$  V is applied across the thickness of top and bottom piezoelectric actuators, respectively, and the static deflection of the plate is calculated by the proposed finite-element model. Figure 3(a) shows the deflection along the centreline of cantilever plate due to the voltage applied to the actuators. The abscissa represents distance measured along the centreline from the fixed end of the beam. Second, the deflection of the plate is calculated for different applied voltages extending from 0 to 60 V. Figure 3(b) shows the deflection of the centreline’s free end point. It can be seen in Figures 3(a) and (b) that the results produced by finite element model meet exactly with referred analytical results.

Finally, the actuator’s effect on the shape control is investigated. The originally flat plate is first subjected to a uniformly distributed load of  $100$  N/m<sup>2</sup> so as to produce initial bending in it. Then to flatten the plate again, active voltage is input incrementally until the centreline deflection of the plate is reduced to a desired tolerance. Figure 3(c) shows the calculated centreline deflection of the composite plate subjected to uniformly distributed load under three different input voltages viz. 0, 30 and 50 V. The results obtained by finite element model are in agreement with the analytical results referred.

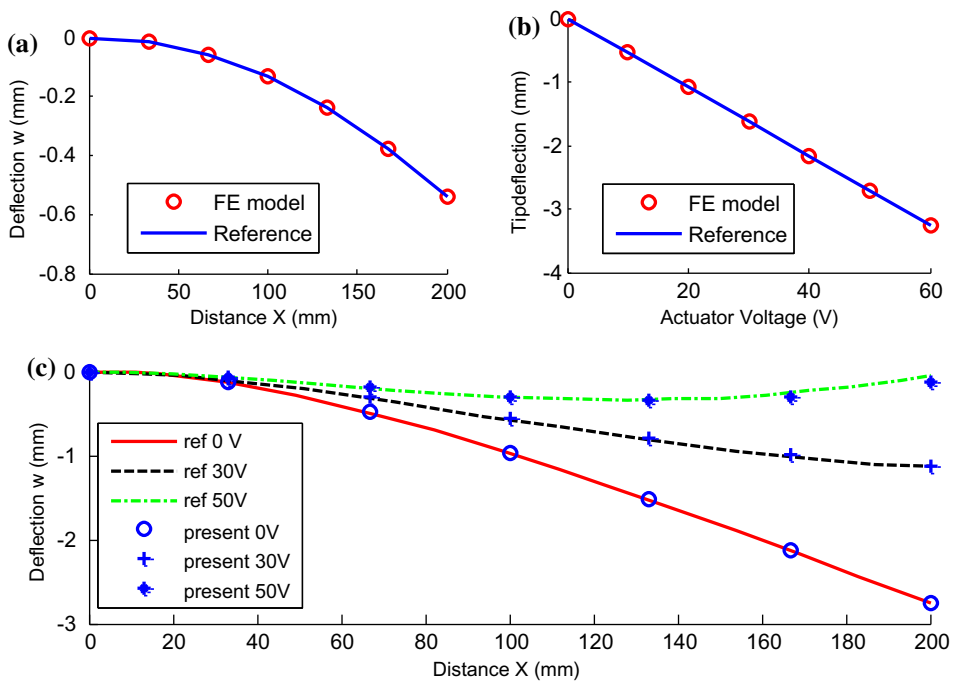


Figure 3. (a) Centerline deflection of the plate (actuator input voltage = 10 V). (b) Deflection of free end point against actuator input voltage. (c) Centerline deflection under uniform load and different actuator input voltages Lam et al. (1997).

### 3.2. Active shape control of paraboloidal antenna reflector

A doubly curved shallow paraboloidal antenna reflector made of laminated [90/0/90] composite (carbon–epoxy) is considered for numerical investigation. The antenna reflector with height  $h = 0.0583$  m, radius  $R = 0.2023$  m and thickness 3.75 mm is considered. It consists of a small circular cut-out of 0.3 around the apex for mounting. For the actuation of the antenna reflector, eight piezo patches are bonded along the meridians separated by  $90^\circ$ , respectively, in a bi-morph arrangement and thus forming four actuators as shown in Figure 4. Thickness of each piezo patch is 1.3 mm. Equal voltages with opposite signs are applied across the thickness of the outer and inner piezoelectric actuators, respectively. The properties of the unidirectional composite (carbon–epoxy) of which host structure is formed and the piezoelectric materials chosen for the study are shown in Table 1.

### 3.3. Beam shaping of antenna reflector

Beam shaping performance characteristics of antenna reflector are highlighted in this section. Beam shaping means widening or narrowing the main beam. It is used when there is a need for change in coverage area of antenna reflector. For the paraboloidal antenna reflector shown in Figure 4, this can be achieved by applying equal voltage of opposite sign at inner and outer piezo-layers to all actuators. Because of symmetric loading and geometry, a quarter of the antenna reflector is modelled as shown in Figure 5(a) and a mesh has been generated using  $10 \times 16$  degenerated shell elements. Piezo-patches are placed as shown in Figure 5(a). When the voltage of 300 V (assuming maximum operating range that can be taken by PZT patch is  $\pm 300$ V) is applied to top layer piezoelectric actuator and  $-300$  V to bottom layer piezoelectric actuator, outward deformation is obtained whereas when the voltage of  $-300$  V is applied to top layer piezoelectric actuator and 300 V to bottom layer piezoelectric actuator, inward deformation is obtained. Resulting deflections (scaled by a factor of 20 for clarity) along the edges AOC and BOD are plotted in Figure 6(a) and (b), respectively. It is observed that all points A, B, C, D move outward or inward. This type of deformation is useful in changing the coverage area of antenna.

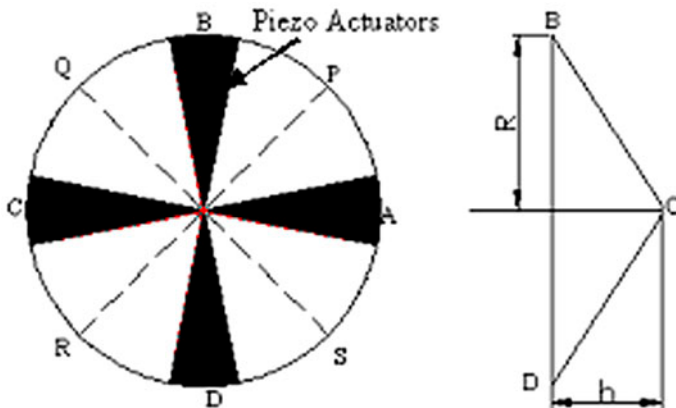


Figure 4. Piezo-laminated paraboloid in bimorph arrangement.

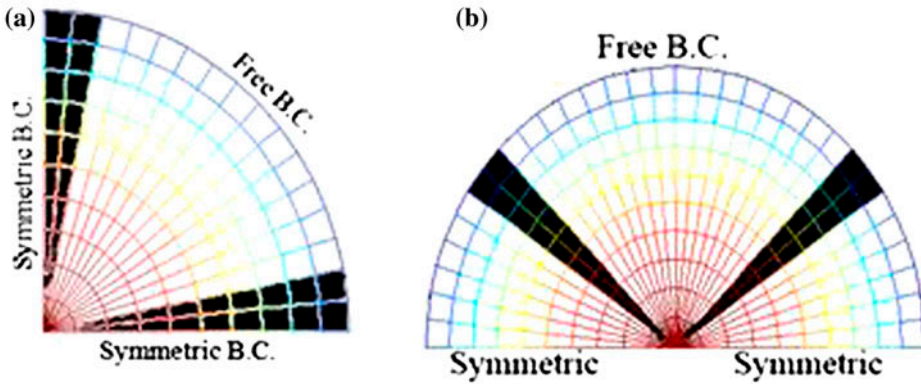


Figure 5. Typical finite element model with piezoelectric patches. (a) Quarter part used to achieve beam shaping. (b) Half part used to achieve beam steering.

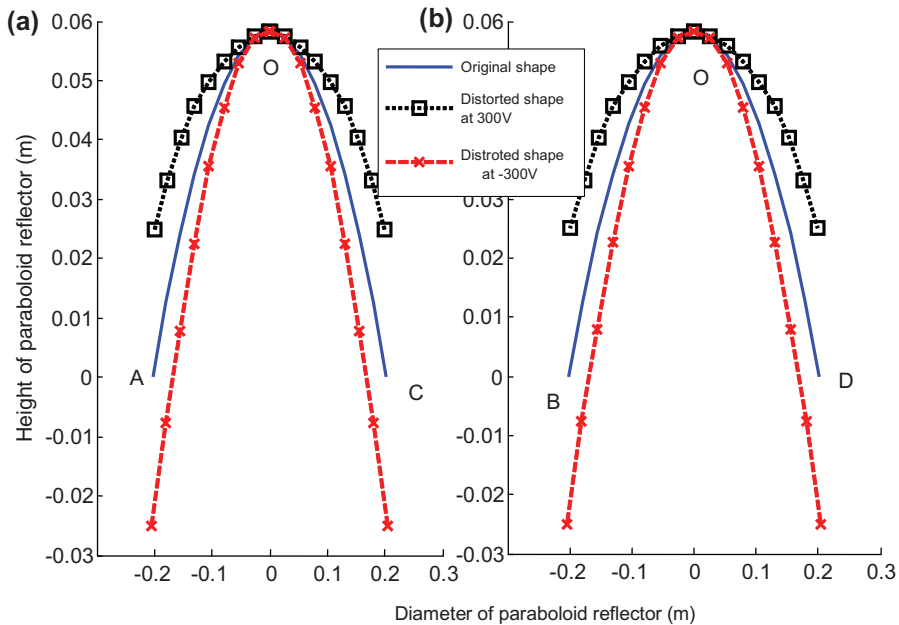


Figure 6. Change in shape of the antenna reflector as required for beam shaping under the applied voltage ( $\pm 300$  V) on the PZT patches (scaled by a factor of 20) (a) along the edge AOC (b) along the edge BOD.

Beam shaping of antenna reflector is further studied using two other piezoelectric materials which are lead-free. Piezoelectric properties of these materials are shown in Table 1. For clarity resulting deflection obtained at 300 V is scaled by a factor of 20 and their comparison with PZT is shown in Figure 7. It is found that deflection obtained in case of PZT is maximum when compared with others.

### 3.4. Beam steering of antenna reflector

Beam steering is another performance characteristic which refers to changing the principal direction of the antenna reflector and is used when one needs to change the scanning area from one location to another location. For the paraboloidal antenna reflector shown in Figure 4, this can be achieved by applying opposite voltage to pairs (viz. (A, B) & (C, D)) of piezoelectric actuators. In this study, for pair (A, B) +300 V is applied to top layer of piezoelectric actuator and -300 V is applied to bottom layer of piezoelectric actuator whereas for pair (C, D), -300 V is applied to top layer piezoelectric actuator and +300 V is applied to bottom layer of piezoelectric actuator. For this case, geometry is symmetric about AC and BD but loading is not symmetric about either AC or BD. However, loading is symmetric about PR as shown in Figure 4, therefore half part of paraboloid shell is modelled as shown in Figure 5(b). Resulting deflection (scaled by a factor of 20 for clarity) along the edge AOC is plotted in Figure 8(a). Steering in opposite direction can be obtained if opposite voltage is applied to the pair (A, B) and (C, D) as depicted in Figure 8(a). It is observed that points A, B, C, D move in such a way that the reflector rotates about its axis. This type of deformation changes the principal direction and hence is suitable for beam steering.

Beam steering of antenna reflector is further studied using two other piezoelectric materials namely KNLNTS and BNK-LBT which are lead-free. The same geometry and loading conditions, as used for PZT, are used for these materials too. A comparative plot of deflections achieved with these materials has been shown in Figure 8(b). For clarity resulting deflections are scaled by a factor of 20. It is observed that deflection of rotation axis obtained in case of PZT is maximum when compared with others. However, KNLNTS gives the performance very near to PZT. Thus, KNLNTS can become a possible replacement for PZT.

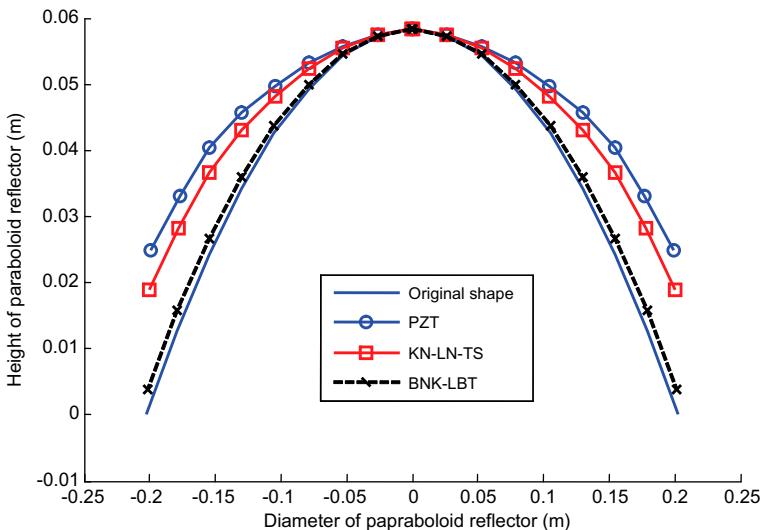


Figure 7. Change in shape of antenna reflector as required for beam shaping under the applied voltage of 300 V for various piezoelectric materials (scaled by a factor of 20).

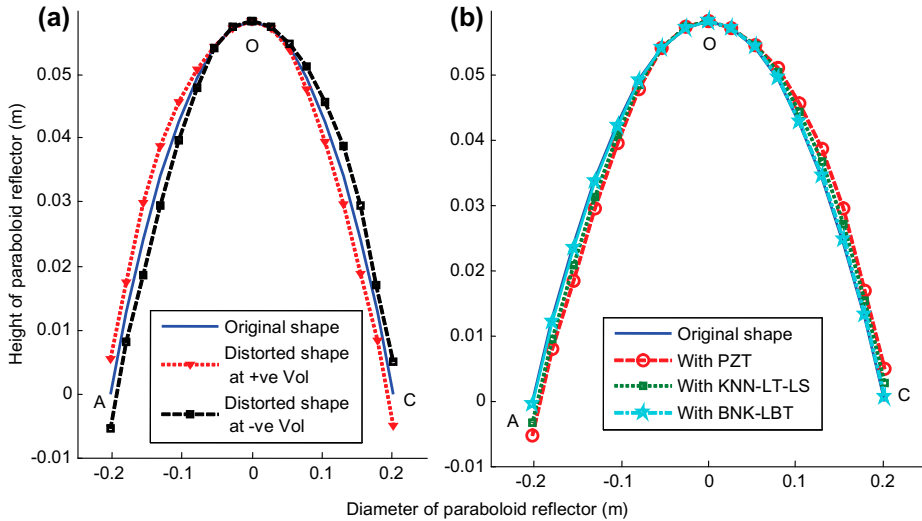


Figure 8. Change in the shape of antenna reflector as required for beam steering at  $\pm 300$  V (a) along edge AOC for PZT (b) along edge AOC for various piezoelectric materials, (scaled by factor 20).

### 3.5. Active shape control under thermal loading

The antenna reflectors are exposed to severe space environment with wide temperature variation from  $-80$  to  $+180$  °C which causes distortion in the original shape leading to weak performance. The model has been analysed by assuming that a linear thermal gradient acts across the thickness of the antenna reflector with a temperature of  $25$  °C on the outer surface and a temperature of  $20$  °C on the inner surface. Due to symmetry in geometry of antenna reflector and thermal conditions, quarter part is considered for the analysis. Initially, to regain the shape, various locations and number of patches are tried randomly and the calculations are done until the local displacement along AOC is reduced to a desired tolerance. Figure 9 shows the location and number of patches which regain the shape to a desired tolerance. Equal voltage is input incrementally to each actuator. Figure 10 shows the resulting local deformation along AOC. The original undeformed shape is kept as datum and thus it appears as a straight line of zero deformation. From the graphs it can be seen that after thermal loading, the highest deformation in the range  $3.4e-5$  is achieved near the free end of antenna reflector. Shape control achieved by applying  $40$ ,  $70$  and  $100$  V has also been shown. Although an applied voltage of  $100$  V brings most of the surface of the deformed antenna reflector back to nearly original shape yet at the end negative deformation is observed which is considerably high. This indicates a need for proper optimisation of dimensions and locations of piezoelectric patches and the voltage applied so as to achieve better shape control.

Before taking up the optimisation the performance of the other two lead-free materials (KNN-LT-LS and BNK-LBT) for active shape control of antenna reflector with the model shown in Figure 9 has been studied. Considering that the best results are obtained at  $100$  V for PZT, performance of the other two materials has first been studied at the same voltage and the comparative plot of all the materials has been depicted

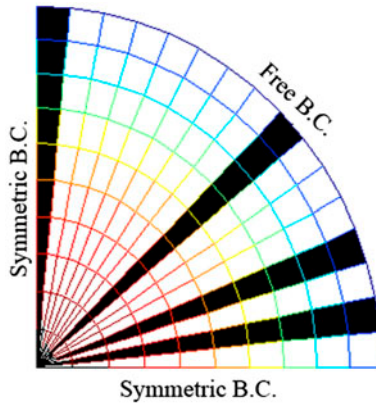


Figure 9. Finite element model with quarter part of paraboloidal antenna reflector showing locations of piezoelectric patches for thermal shape control.

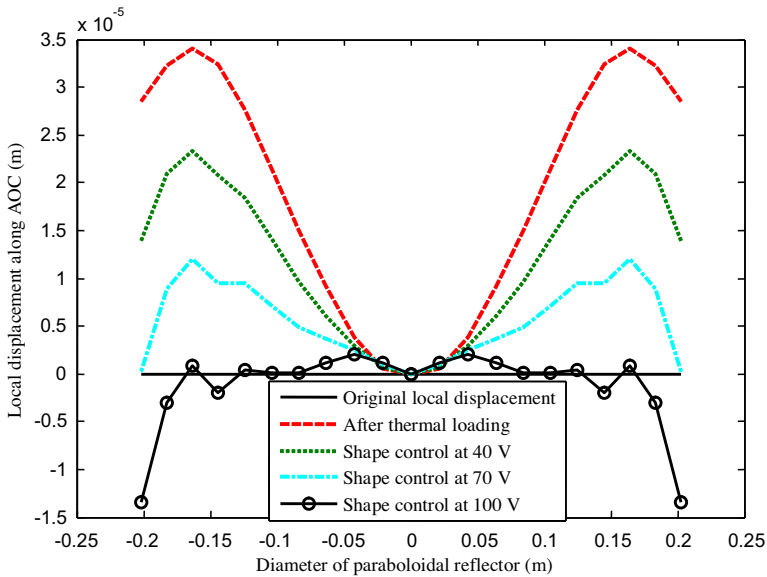


Figure 10. Deformation after thermal loading and regain of the shape with application of different voltage to piezo-patches (along the edge AOC).

in Figure 11. It is found that shape regain of reflector is best for PZT followed by KNLNTS and BNK-LBT, respectively, when applied voltage is 100 V. Now, the finite element model has been used to find out the voltage at which KNLNTS gives best shape control as shown in Figure 12. It is found that for KNLNTS-based piezoelectric material the original shape of antenna reflector has been obtained at 200 V. Although there is a significant increase in voltage, lead-free piezoelectric patches can be used in order to overcome the harmful effects of lead-based piezoelectric patches. Therefore, in the case where use of lead-free material is of prime importance KNLNTS-based piezoelectric material can be used instead of PZT.

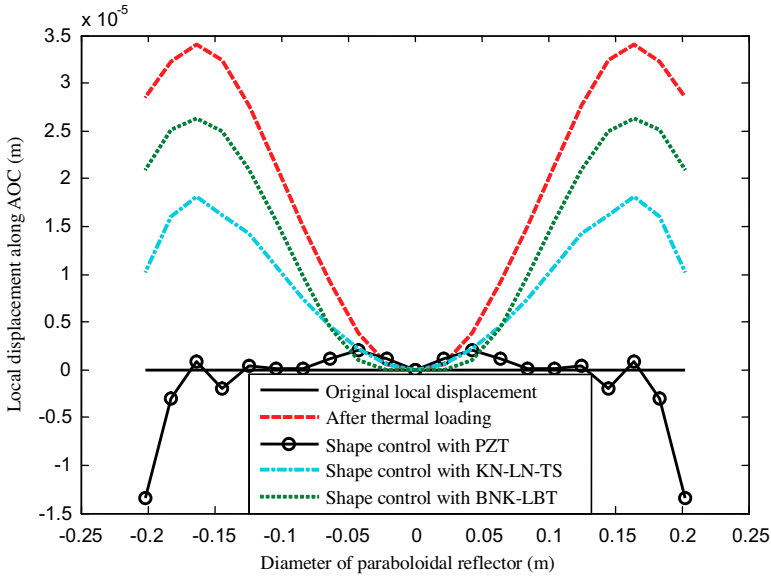


Figure 11. Shape control of antenna reflector achieved by applying 100 V to different piezoelectric materials.

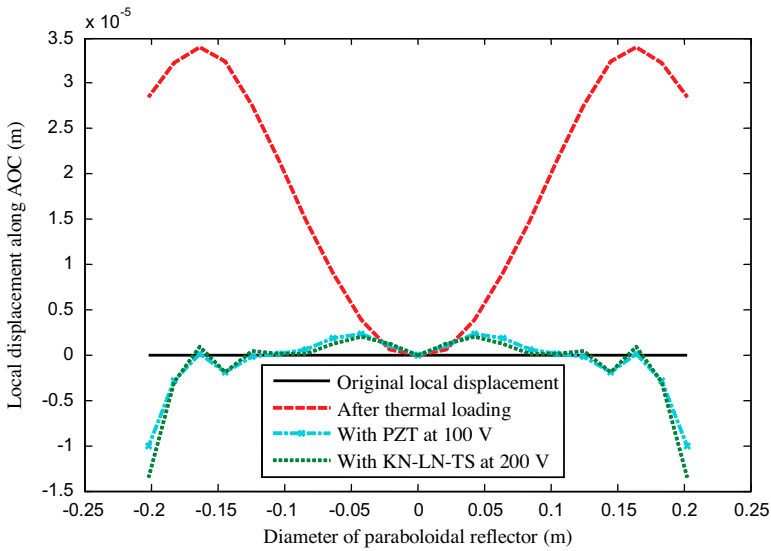


Figure 12. Shape control of antenna reflector obtained by applying 100 V to PZT patches and 200 V to KNLNTS patches.

**3.6. Voltage and patch location optimisation**

In this section, to regain the original shape of distorted paraboloid antenna under thermal load, optimised locations and lengths of patches along with optimised voltage for each patch are obtained. Discrete piezoelectric patches that cover full element have been

considered for this purpose. Figure 14(a) shows the quarter part of the paraboloidal antenna with original as well as distorted shape due to thermal loading. For this case, a stochastic optimisation method such as GA is more useful for the optimisation when compared to gradient-based technique. The reason being that the gradient-based techniques begin their search for solution in the neighbourhood and if there are more than one local minimum or maximum, then it may not find the correct global optimum. This problem does not arise with GA as it uses function values instead of function derivatives and searches for optimal values almost randomly in a broad search space. GA starts with initial population of random numbers based on individual variables. It uses the fitness value for each random number of the chosen population using the objective function which is to be optimised. Then, processes such as reproduction, crossover and mutation are used to obtain new population. This process of generation of new population continues until maximum number of generations is reached or optimal values have reached their tolerances. The flow chart of optimisation procedure using GA is shown in Figure 13.

The shape of antenna reflector is principally outlined by the shape of its mid-plane. Thus, after meshing it is defined by the displacement of the nodes on the mid-plane. Also, the induced deflection due to the piezoelectric actuators is dependent on geometry, material properties of actuator, the applied voltage, the length and number of piezoelectric actuators. Therefore, an error between achieved shape and desired shape is

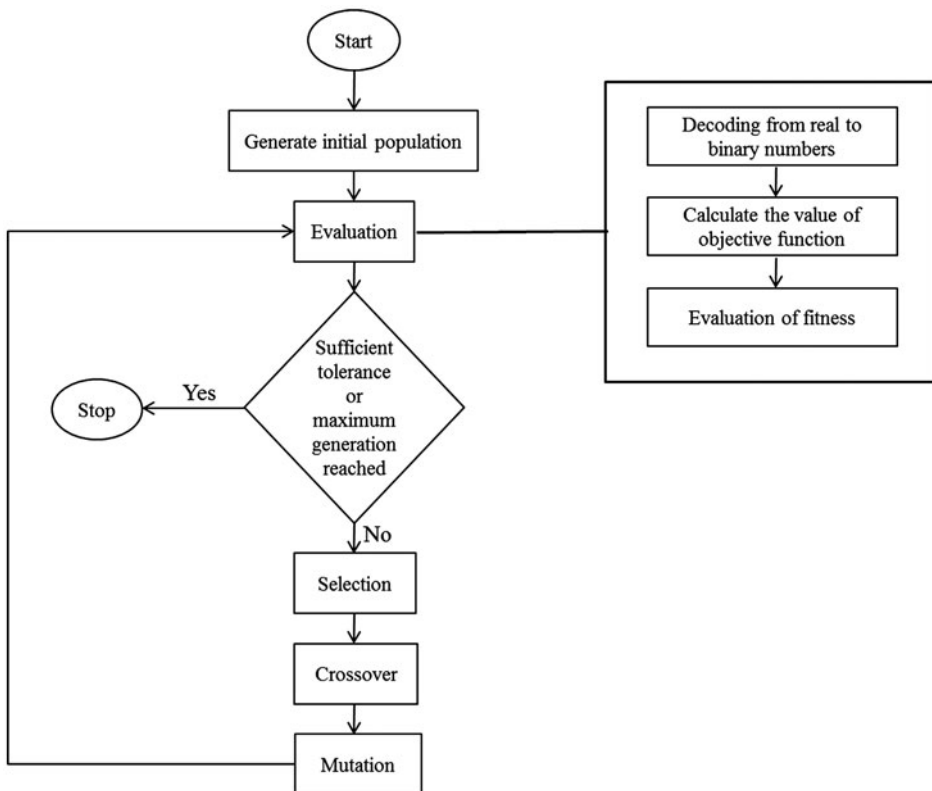


Figure 13. The flow chart of optimization procedure using GA.

considered as the objective function for the optimisation problem and can be defined as the sum of the squares of the deviation in desired displacement and achieved displacement at all the nodes.

$$\text{error} = \sum_{i=1}^{\text{nnode}} \left( (u_{d_i} - u_i)^2 + (v_{d_i} - v_i)^2 + (w_{d_i} - w_i)^2 \right)$$

where nnode = number of nodes

$u_{d_i}, v_{d_i}, w_{d_i}$  = Desired deflection at node  $i$

$u_i, v_i, w_i$  = Achieved deflection at node  $i$

For the optimal shape control of antenna reflector, it is desired to minimise the error by finding the set of optimal parameters. In order to obtain this, there will be a lower and upper bound constraint on these parameters which are to be optimised. Therefore, putting together these constraints the optimisation problem can be defined as:

$$\begin{aligned} &\text{min, error} \\ &\text{subjected to} \\ &c_{\min} \leq c \leq c_{\max} \end{aligned}$$

where  $c_{\min}$  and  $c_{\max}$  are the minimum (lower bound) and maximum (upper bound) constraints applied on various parameters such as patch location and size, and voltage.

The parameters used for optimisation are location and size of actuators and the voltage applied to actuators. The locations of piezoelectric patches are constrained to lie between 1 and total number of elements. The lengths of patches are constrained to lie between 1 and maximum number of elements in meridional direction whereas the width of patches is kept fixed to one element only. The voltages are constrained to be in the range of 0–300 V. A total of six patches have been used in this case. Different values of mutation and crossover probabilities were tried in GA and finally a mutation probability of .02 and crossover probability of .80 were selected for the population size of 200. Optimum voltage and patch locations are shown in Table 2, which are graphically shown in Figure 14(b). Figure 15(a) shows the deflection along AOC with respect to the original shape. The original un-deformed shape is kept as datum and thus it appears as a straight line of zero deformation in Figure 15(a). The curve with the dashed lines represents the deflections along edge AOC after the thermal loading. The dotted curve overlapping the original shape straight line represents the final deflections along edge AOC after the optimised control voltage is applied to the thermally distorted shape. It is clear from Figure 15(a) that the optimisation has enabled nearly 100% regain of the original shape.

Active shape control of antenna reflector is further studied for other piezoelectric material KNLNTS which is lead-free. Optimum voltage and patch locations when

Table 2. Optimised voltage applied to individual patch (for PZT).

Patch No.	Patch locations						Voltage (V)
1	35	36	37	38	39	40	48.84930
2	103	104	105	106			63.50481
3	58						32.12093
4	1	2	3	4	5		1.00043
5	68						1.00000
6	135	136	137	138			98.84162

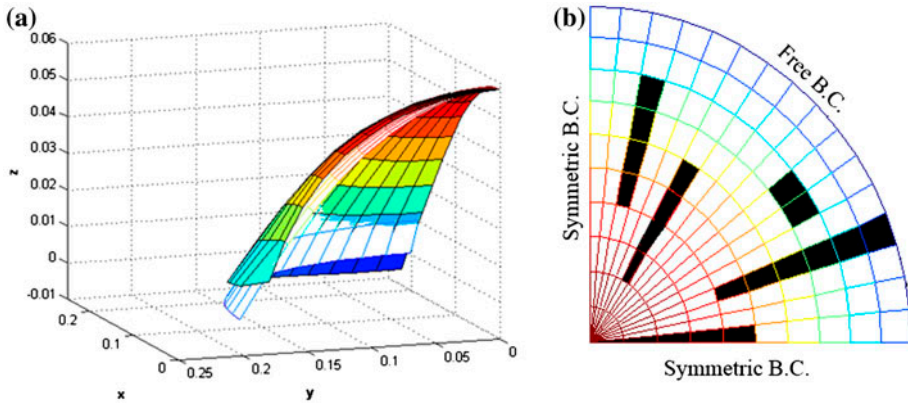


Figure 14. (a) Deformed (dark) and un-deformed (light) shape of quarter part of antenna reflector under thermal loading. (b) PZT piezoelectric patches at optimum locations on the quarter part of antenna reflector.

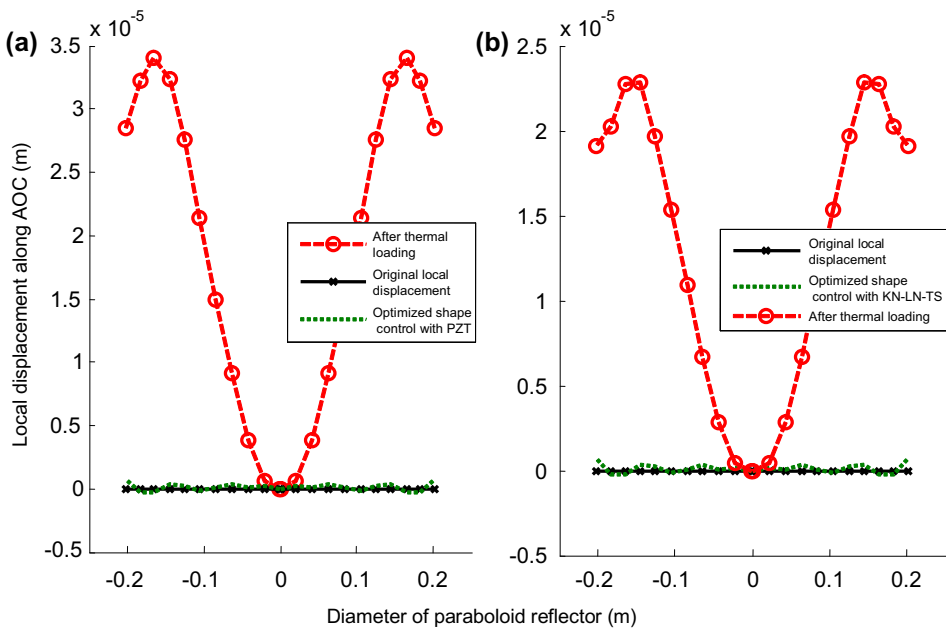


Figure 15. (a) Shape control achieved by applying optimised voltage to (a) PZT patches at optimised locations (b) Lead free KNLNTS patches at optimised locations.

KNLNTS is used are shown in Table 3. Figure 15(b) shows the deflection along AOC with respect to the original shape. The dotted curve overlapping the original shape straight line represents the final deflections along edge AOC after the optimised control voltage is applied to the thermally distorted shape. Thus, Figure 15(b) shows that nearly 100% regain of the original shape can be achieved using KNLNTS as well when proper optimisation for the locations and sizes of the actuators and the voltage applied

Table 3. Optimised voltage applied to individual patch (for KN-LN-TS).

Patch No.	Patch locations					Voltage (V)
1	77	78	79	80		99.07045
2	102	103	104			136.61699
3	145	146	147			159.98261
4	125	126	127	128	129	127.31464
5	156	157	158	159	160	118.04221
6	93	94	95	96	97	113.45563

to the actuators is done. Although a significant increase in the voltages applied is observed (Tables 2 and 3) when KNLNTS actuator patches are used instead of PZT actuator patches yet in order to overcome the harmful effects of lead-based piezoelectric patches KNLNTS can successfully be used as a lead-free material for the active shape control.

#### 4. Conclusions

Piezo-thermo-elastic laminated shell has been modelled and analysed using finite element method. Beam shaping and beam steering phenomena of antenna reflector as well as shape control of antenna reflector have been demonstrated. Performance of lead-free piezoelectric materials KNLNTS and BNK-LBT has been compared with the performance of lead-based PZT for beam shaping, beam steering and shape control of antenna reflector. It is observed that best performance is achieved by using PZT when compared with other two materials. However, if it is required to use lead-free materials then KNLNTS can be used as an alternative. Further optimisation has been done for sizes and locations of piezoelectric patches and the voltage applied. It has been demonstrated that optimised sizes and locations of piezoelectric patches along with optimised voltage applied can efficiently cancel off the thermal distortion of antenna reflector. Efficient shape control has been demonstrated using lead-free piezoelectric material KNLNTS though voltage applied is higher for this when compared to PZT.

#### Acknowledgement

Rahul Vaish acknowledges DST, New Delhi, India for financial support through INSPIRE Faculty Award-2011.

#### References

- Agrawal, B. N., Elshafei, A. A., & Song, G. (1997). Adaptive antenna shape control using piezoelectric actuators. *Acta Astronautica*, 40, 821–826.
- Agrawal, B. N., & Treanor, K. E. (1999). Shape control of a beam using piezoelectric actuators. *Smart Materials and Structures*, 8, 729–740.
- Aksel, E., & Jones, J. L. (2010). Advances in lead-free piezoelectric materials for sensors and actuators. *Sensors*, 10, 1935–1954.
- Chan, H. L. W., Choy, S. H., Chong, C. P., Li, H. L., & Liu, P. C. K. (2008). Bismuth sodium titanate based lead-free ultrasonic transducer for microelectronics wire bonding applications. *Ceramics International*, 34, 773–777.
- Detwiler, D. T., Shen, M. H. H., & Venkayya, V. B. (1995). Finite element analysis of laminated composite structures containing distributed piezoelectric actuators and sensors. *Finite Elements in Analysis and Design*, 20, 87–100.

- Gupta, V. K. (2011). Modified approach for optimum position and sizing of piezoelectric actuator for steering of parabolic antenna. *Tech Science Press*, 6, 65–75.
- Haftka, R. T., & Adelman, H. M. (1985). An analytical investigation of shape control of large space structures by applied temperatures. *American Institute of Aeronautics and Astronautics Journal*, 23, 450–457.
- Irschik, H. (2002). A review on static and dynamic shape control of structures by piezoelectric actuation. *Engineering Structures*, 24, 5–11.
- Koconis, D. B., Kollar, L. P., & George, S. (1994). Shape control of composite plates and shells with embedded actuators-II, desired shape specified. *Journal of composite materials*, 28, 262–285.
- Kumar, R., Mishra, B. K., & Jain, S. C. (2008). Vibration control of smart composite laminated spherical shell using neural network. *Journal of Intelligent Materials and Structures*, 19, 947–957.
- Lam, K. M., Peng, P. Q., Liu, G. R., & Reddy, J. N. (1997). A finite-element model for piezoelectric composite laminates. *Smart Materials and Structures*, 6, 583–591.
- Lee, T., Kwok, K. W., Li, H. L., & Chan, H. L. W. (2009). Lead-free alkaline niobate-based transducer for ultrasonic wire bonding applications. *Sensors and Actuators, A: Physical*, 150, 267–271.
- Maeder, M. D., Damjanovic, D., & Setter, N. (2004). Lead free piezoelectric materials. *Journal of Electroceramics*, 13, 385–392.
- Takenaka, T., Nagata, H., & Hiruma, Y. (2008). Current developments and prospective of lead-free piezoelectric ceramics. *Japanese Journal of Applied Physics*, 47, 3787–3801.
- Washington, G. (1996). Smart aperture antennas. *Smart Materials and Structures*, 5, 801–805.
- Yasuyoshi, S., Hisaaki, T., Toshihiko, T., Tatsuhiko, N., Kazumasa, T., & Takahiko, H. (2004). Lead-free piezoceramics. *Nature*, 432, 84–86.
- Yoon, H. S., & Washington, G. (1998). Piezoceramic actuated aperture antennae. *Smart Material and Structures*, 7, 537–542.
- Yoon, H. S., Washington, G., & Theunissen, W. H. (2000). Analysis and design of doubly curved piezoelectric strip-actuated aperture antennas. *IEEE Transactions on Antennas and Propagation*, 48, 755–763.